Understanding the AIE phenomenon of nonconjugated rhodamine derivatives through a new viewpoint of symmetry breaking

Lin-Lin Yang[1,2,5], Haoran Wang[2,3,4,5], Jianyu Zhang[3], Qiyao Li[2], Jie-Ying Chen[1], A-Ling Tang[1], Jacky W. Y. Lam[3], Zheng Zhao[2,4,*], Song Yang[1,*], and Ben Zhong Tang[2,3,4,*]

Affiliations

[1]National Key Laboratory of Green Pesticide, Key Laboratory of Green Pesticide and Agricultural Bioengineering, Ministry of Education, Guizhou University, Huaxi District, Guiyang 550025, China.

[2]School of Science and Engineering, Shenzhen Institute of Aggregate Science and Technology, The Chinese University of Hong Kong, Shenzhen, Guangdong 518172, China.

[3]Hong Kong Branch of Chinese National Engineering Research Center for Tissue Restoration and Reconstruction, Department of Chemistry, and Guangdong-Hong Kong-Macao Joint Laboratory of Optoelectronic and Magnetic Functional Materials, The Hong Kong University of Science and Technology, Clear Water Bay, Kowloon, Hong Kong, 999077, China.

[4]HKUST Shenzhen Research Institute, No. 9 Yuexing 1st RD, South Area Hi-tech Park, Nanshan, Shenzhen, 518057, China.

[5]These authors contributed equally: Lin-Lin Yang, Haoran Wang.

*Correspondence authors: zhaozheng@cuhk.edu.cn, jhzx.msm@gmail.com and tangbenz@cuhk.edu.cn.

TOC Graphic
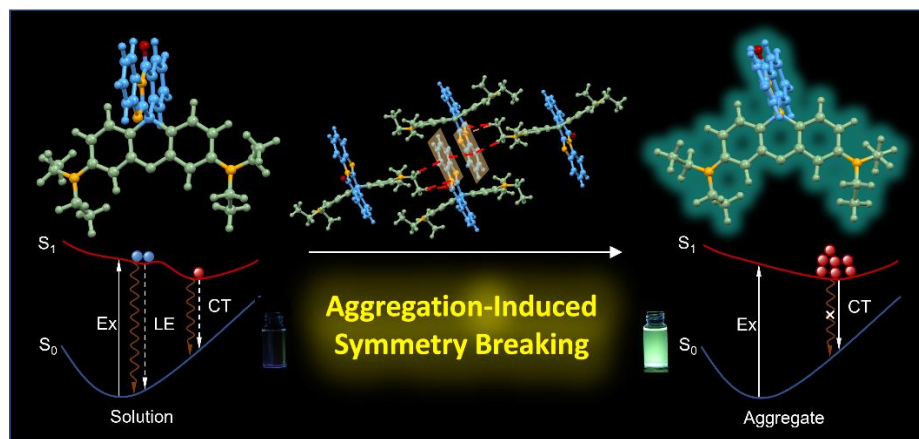
Abstract

Solid-state emissive materials are of great importance due to their wide applications in the field of bioimaging and optoelectronic devices. The concept of aggregation-induced emission (AIE) provides a reliable strategy to afford solid-state emissive luminogens with the guidance of restriction of intramolecular motion (RIM) mechanism. Traditional AIE luminogens (AIEgens) exhibit enhanced emission intensity under increased viscosity or decreased temperature, attributed to the RIM mechanism. However, some luminogens were found without the classic viscosity or temperature effect, but still display AIE feature. In this work, we synthesized a series of cross-shaped and closed-form rhodamine-based unorthodox AIEgens. Their abnormal emission behavior in increased viscosity and cooling experiments suggested that their strong solid-state luminescence (up to 72.7%) was not ascribed to the conventional RIM working mechanism. Through a systematical investigation including single-crystal structural analysis, optical property study and theoretical calculations, we proposed that aggregation-induced symmetry breaking (AISB) may induce intramolecular charge transfer and act as a general principle to dominate the unique aggregate-state emission behavior of the nonconjugated rhodamine derivatives. More importantly, AISB not only provides a feasible approach for the design of unique rhodamine-based AIEgens, but also helps us deeply understand the change of luminescent behavior of materials upon aggregation with a wide perspective.

Introduction

Symmetry and asymmetry are of great significance for our deep understanding of nature.[1,2] The early study of symmetry and symmetry breaking can go back to Pierre Curie.[3] And it was first predicted in a famous paper on the violation of the parity law in

weak interactions, by Nobel prize in Physics 1957 awardees Chen Ning Yang and Tsung-Dao Lee. Since then, it has been gradually realized that symmetry breaking has a tight relationship with mathematics, physical theory, and even the philosophy of science. Symmetry breaking also creates the universe and life.[4] Though molecules can take both "left-handed" and "right-handed" forms, life originates from left-handed amino acids and living organisms predominately use right-handed sugars.[5,6] For macroscopic materials, the diversity of their properties possibly originates from symmetry breaking, including antiferromagnets, ferroelectrics, liquid crystals, etc.[7,8,9,10,11,12,13] Therefore, symmetry breaking has important implications for the origins of life, scientific research, as well as understanding and manipulating the properties and applications of materials.[14,15,16]

The method of studying phases and transitions in terms of symmetry and symmetry breaking is known as the Landau paradigm, in which aggregates are involved.[17,18] Aggregate is one of the common existing forms of macroscopic materials, as anything above a single molecular specie can in principle be deemed as aggregate.[19] It has turned out that the behavior of large and complex aggregates composed of elementary units cannot be understood in terms of simple accumulation of the properties of these particles.[20] That is, the whole becomes not only more than the sum of its parts, but very different from the sum of its parts.[21,22] Specifically, molecules in the gas or liquid phase exhibit a disordered arrangement, displaying single molecular properties. While in the crystal state, molecules display anisotropy with an ordered packing, leading to property transition (Scheme 1a).[23,24] For example, the varied properties of water and ice are assigned to the symmetry decrease of isotropy of water molecules from the liquid state to the solid state (Scheme 1b). Besides the above-mentioned newly emerged properties

of aggregates compared to their single molecular species, the subtle difference in packing mode/ assembly size/ morphology among aggregates with the same composition can also result in varied properties and functions.[25,26,27,28,29] In this regard, aggregation-induced emission (AIE) is a symbolic and well-studied case, which refers to the photophysical behavior of organic molecules displaying weak or no emission in dilute solutions but much enhanced emission in the aggregate state (Scheme 1b).[30] The working mechanism of AIE is proposed to be the restriction of intramolecular motion (RIM), which claims that the active excited-state intramolecular motion in the solution state facilitates the non-radiative decay and thus quenches the emission while the aggregation can restrict the excited-state intramolecular motion and thus suppress the non-radiative decay to light up the emission.[31,32,33] Based on the investigation and deep understanding of the AIE phenomenon, research that focuses on the variations of aggregate and their composed units like molecules has attracted great attention and was coined as aggregate science.[34,35,36,37] Within the research philosophy of aggregate science, varied fields including aggregation-induced generation of ROS, photothermal/photoacoustic effects in aggregate, solid-state molecular motion, aggregation-induced chirality, as well as room temperature phosphorescence in aggregate, etc. have gained wide research attention and grown as independent research fields.[38,39,40,41,42,43,44,45,46,47] Nobel prize winner P. W. Anderson pointed out that symmetry breaking was formulated from quantitative to qualitative differentiation in his science paper "More is Different", which underlined the universality of symmetry breaking in complex condensed phases or aggregates.[48] Although symmetry breaking can elegantly explain some common physical property changes at different states, its application in unveiling the optical changes of luminescent

materials at different state are scarcely deeply explored except chirality.[49,50] Therefore, aggregation-induced symmetry breaking (AISB) may have the potential to account for the variations between single molecular state and aggregate state.
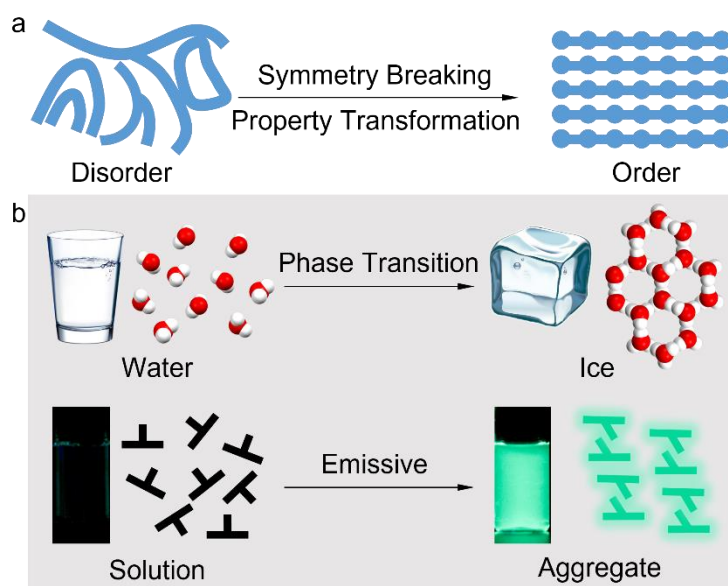
Scheme 1. (a) Schematic illustration of the system from disorder to order packing.(b) Schematic illustration of the crystalization of water molecules (top) and the emission behavior of AIEgens (bottom).

To get an insight into AISB, a series of closed-form rhodamine-based AIE luminogens (AIEgens) were introduced into this work. Traditional rhodamine-based compounds, with a planar π-conjugated xanthene core, are favored with high absorption coefficient, high fluorescence quantum yield, water solubility and biocompatibility. In most cases, turn-on behavior of rhodamine-based compounds from "closed" to "open" form is widely used, working as fluorescent probes and biosensors.[51] However, both closed and open forms were non-emissive in the solid state, thus solid-state fluorescence would expand the potential of rhodamines.[52] A great endeavor has been put to make the rhodamine-based dyes AIE-active by structural modification. The most frequently used method is the

introduction of rotors to the backbone based on RIM working mechanism, such as attaching tetraphenylethene moiety/ planar polycyclic aromatic rings by covalent bonding to the periphery of rhodamine backbones (Scheme 2a).[53,54,55] Although these modifications are effective, they usually suffer from complicated molecular design, rigorous synthetic conditions, and tedious organic synthesis. Different from the previous work, we creatively modified the backbone structure by simple synthesis, successfully generating AIE-active rhodamine-based compounds with cross-shaped six-membered structure, as shown in Scheme 2b. Through systematic study, we found that their AIE properties could be understood from a new viewpoint of AISB other than the conventional RIM. Food spoilage detection of seafood was also realized, showing their promising prospect for portable prototypes.

Results

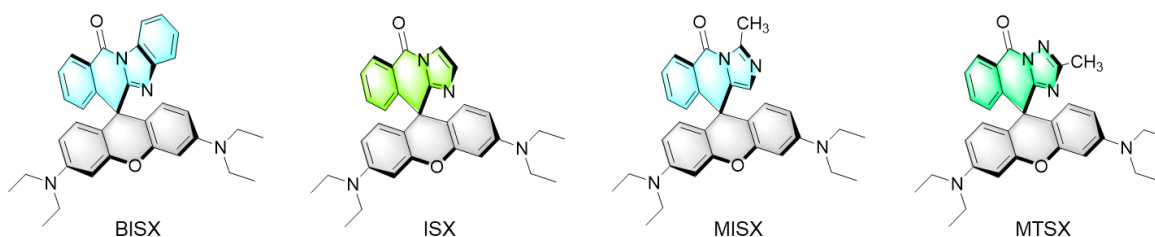## Structures and photophysical properties

a. Previous work (AIE active)
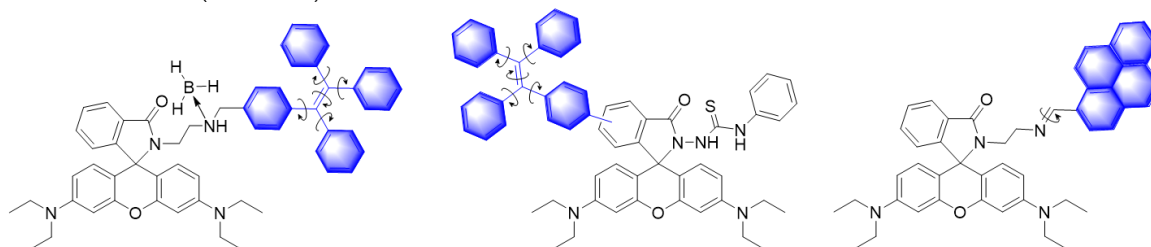
Angew. Chem. Int. Ed. 2016, *55*, 519   *Chem. Sci.* 2017, *8*, 2047   *ACS Appl. Mater. Interfaces* 2017, *9*, 8910

b. This work (AIE active)

Scheme 2. (a) Previously reported work on Rhodamine B-based AIEgens via introducing rotors. (b) Unique rotor-free Rhodamine B-based AIEgens (BISX, ISX, MISX and MTSX) reported in this work.

The target compounds so-named BISX, ISX, MISX and MTSX were readily achieved via a facile synthetic route from their corresponding imidazole or triazole derivatives using the C–N and C–C coupling cyclization reaction with rhodamine B chloride, according to our previous work.[56] Details of the experimental procedures are provided in the Support Information (Scheme S1). DFT calculations were carried out to investigate the reaction mechanism of MISX (Figure S1). All compounds were fully characterized by ^{1}H NMR and ^{13}C NMR spectroscopies, high-resolution mass spectrometry, and the obtained single-crystal structures, respectively (Figure S2-S13, Table S1).

After confirming the structure, we investigated their UV-vis absorption and photoluminescence (PL). As shown in Figure S14, the four compounds displayed similar characteristic absorption spectra with several sharp bands between 240 nm to 330 nm in THF solutions, which could be attributed to their intramolecular n-π* transition and π-π* transition. To explore their AIE feature, PL spectra were measured in THF/water mixtures, respectively (Figure 1a-d). For BISX, when the water fraction was below 80%, it was non-emissive. However, when the water fraction reached 90%, an intensified emission peak at 510 nm emerged. And the emission amplified at f_w = 99% with a 25-fold increase relative to that in THF solution, displaying a bright green fluorescence (Figure 1e). The other three compounds (ISX, MISX and MTSX) showed a similar pattern, with their emission intensity in the aggregate state enhanced to about 35, 80, and 35-fold compared to that of the THF solution, respectively (Figure 1f-h). The aggregate formation was manifested by the level-off tails in the long-wavelength region of the absorption spectra

in the aqueous mixtures due to the Mie effect of the dye nanoparticles (Figure S15). Therefore, all four compounds presented typical AIE features, with aggregates formation confirmed by dynamic light scattering analysis (Figure S16). For all of the four compounds, their lifetimes in the crystal state are one order of magnitude higher than that in the solution state, which matched their enhanced emission from solution to solid state (Figure S17-S20).
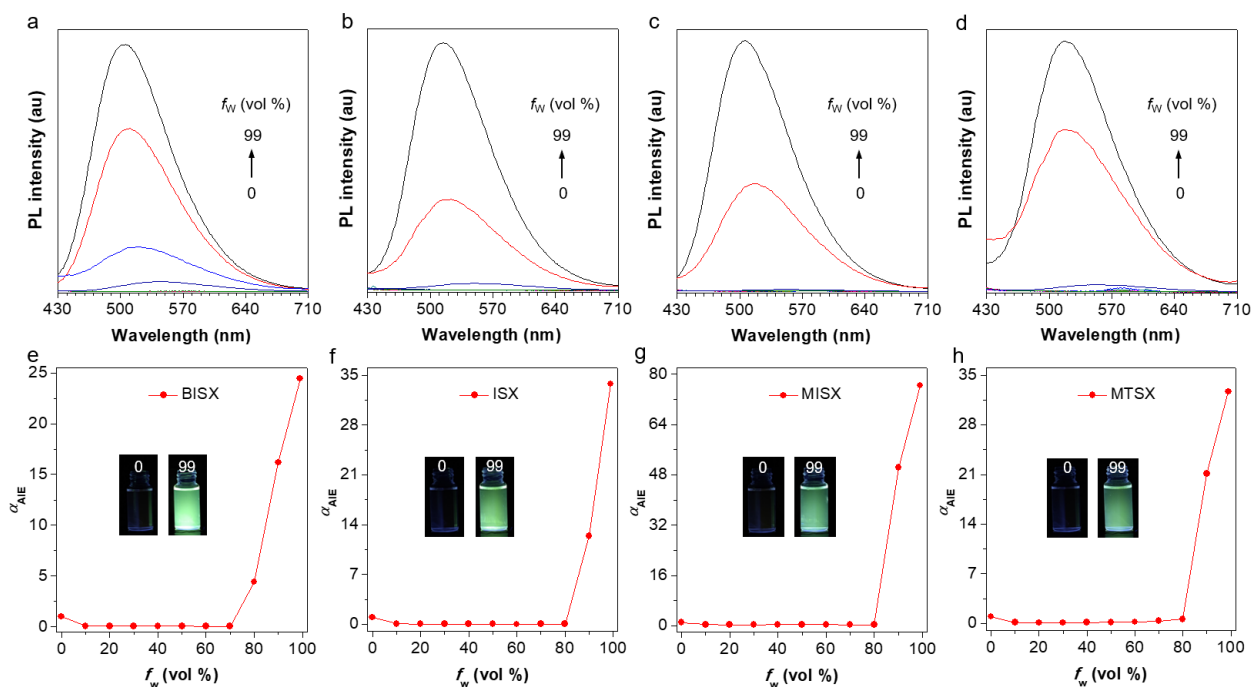

Figure 1. (a-d) PL spectra of BISX, ISX, MISX and MTSX in THF/water mixtures with different water fractions (f_w). c = 1×10^{-5} M, λ_{ex} = 365 nm. (e-h) Plots of relative PL intensity α_{AIE}(I/I_0) versus f_w, where I_0 was the maximal PL intensity in THF solution. Inset: fluorescence images of BISX, ISX, MISX and MTSX in THF/water mixtures with f_w = 0% and 99%, respectively.

Mechanism of AIE study

To disclose the AIE feature of the four compounds, firstly, we measured their emission in the methanol/glycerol mixtures with varied glycerol fractions, since typical AIE molecules generally show enhanced emission in high viscous media due to the RIM mechanism. To

our surprise, for all four compounds, increasing viscosity of the mixture had no impact on the fluorescence intensity (Figure 2a and S21). Then a classical cooling experiment was performed. As shown in Figure 2b and 2c, when gradually decreasing the temperature of BISX dissolved in THF from ambient temperature to -196 °C, its AIE emission peak at 540 nm barely enhanced. Instead, an emission peak at a short wavelength enhanced gradually, and so did the other three compounds (Figure S22). These unexpected phenomena indicated that these AIEgens may not be determined by the conventional RIM working mechanism,[20] further arousing our attention.
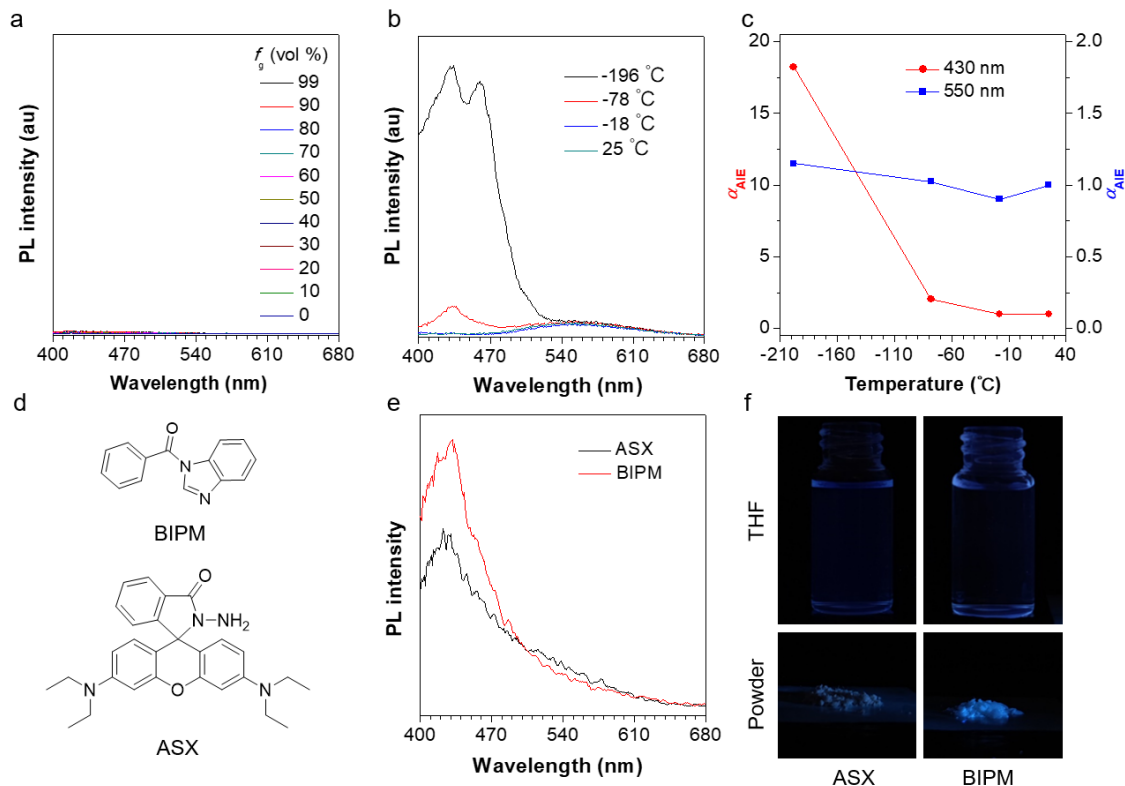
Figure 2. (a) PL spectra of BISX in methanol/glycerol mixtures with different glycerol fractions (f_g). c = 1×10^{-5} M, λ_{ex}= 365 nm. (b) PL spectra of BISX in THF solution with different temperatures. c = 1×10^{-5} M, λ_{ex} = 365 nm. (c) Plots of relative PL intensity α_{AIE} (I/I_0) versus temperature. (d) Chemical structures of BIPM and ASX. (e) PL spectra of BISX, ASX, and BIPM in THF solution. c = 1×10^{-5} M,

λ_{ex} = 365 nm. (f) Fluorescence images of ASX and BIPM in the solution and aggregate state taken under 365 nm UV irradiation.

As these cross-shaped molecules are separated by two moieties, the xanthene part and isoquinolinone part, elucidating which part serves as the chromophore became significant to understand the AIE behavior of this non-typical AIE system. As a result, ASX, an analog of xanthene, was designed and prepared from rhodamine B (Figure 2d, Scheme S2a, Figure S23-S25). A series of compounds, namely BIPM, IPM, MIPM and MTPM, corresponding to the isoquinolinone part of BISX, ISX, MISX and MTSX were also synthesized, respectively (Figure 2d, Scheme S2b, Figure S26-S37). When checking the PL performance of ASX and BIPM, we found both compounds were weakly emissive in the solution and aggregate state, suggesting that the AIE property of BISX originates from neither the upper xanthene core nor the bottom nitrogen heterocyclic part (Figure 2f, Figure S38). It was found that both the emission peaks of ASX and BIPM in THF solutions locate at 430 nm, corresponding to the enhanced emission peak of BISX in THF at low temperature, indicating that decreasing temperature restricted the motion of single molecular species and benefited the emission of the localized emission of upper (isoquinolinone) or bottom (xanthene) moieties (Figure 2e). Same conclusions were also drawn for compounds ISX, MISX and MTSX (Figure S38). Then we assumed that their AIE behavior may result from the new chromophore generated by intermolecular through-space interactions after aggregation. Excitation spectra of the four compounds were measured, respectively (Figure S39-S42). For BISX, one set of peaks appeared between 270 nm and 340 nm, corresponding to its absorption spectrum in Figure S13. Besides, different from its absorption, a weak and broad excitation peak between 350 nm and 400

nm was observed, suggesting some unfavored transition processes may exist within these molecules. The excitation behaviors of ISX, MISX and MTSX were similar to BISX.

To unveil whether the intermolecular through-space interaction is responsible for the aggregate emission of these closed-form rhodamine derivatives, we analyzed the single-crystal structures of the four compounds. The single crystals of BISX, ISX and MTSX were obtained by slow evaporation of their acetonitrile solutions, respectively, while the single crystal of MISX was grown from its acetonitrile-water (4:6, v/v) mixtures. For BISX crystal, except for short contacts including hydrogen bonding and C-H···π interactions, π-π interactions at the distance of 3.359 Å were also found between the benzo-imidazole rings (Figure 3a and S43). These intermolecular interactions may facilitate the restriction of molecular motion of BISX, thus inhibiting the nonradiative decay. And intermolecular π-π interactions may benefit the formation of the chromophore to induce its AIE property. Interestingly, ISX crystal, with only hydrogen bonds (2.340 Å and 2.976 Å) and C-H···π interactions (2.837 Å and 2.806 Å) rather than π-π interactions, also exhibited similar AIE behavior like BISX (Figure S44 and Figure 3b). As for MISX crystal, C-H···π interactions with the distance of 2.892 Å were observed (Figure S45). Though hydrogen bonding interactions (C-H···O) with the distance of 2.596 Å between two isoquinolinone rings could be found, there was no observable π-π interaction. Staggered packing was observed for the two rings, similar to ISX (Figure 3c). MTSX crystal also possessed π-π interactions, analogous to BISX (Figure 3d and S46). Therefore, comparing the packing mode of BISX and ISX crystal, and MISX and MTSX, we concluded that intermolecular through-space interaction did not necessitate the chromophore formation and the AIE properties of these rhodamine derivatives. To further verify our proposal, non-covalent

interactions were calculated by reduced density gradient (RDG) method.[57] As shown in Figure 3e-h, substantial intermolecular through-space interactions were found for BISX and MTSX, while ISX and MISX exhibited negligible intermolecular interactions. Thus,
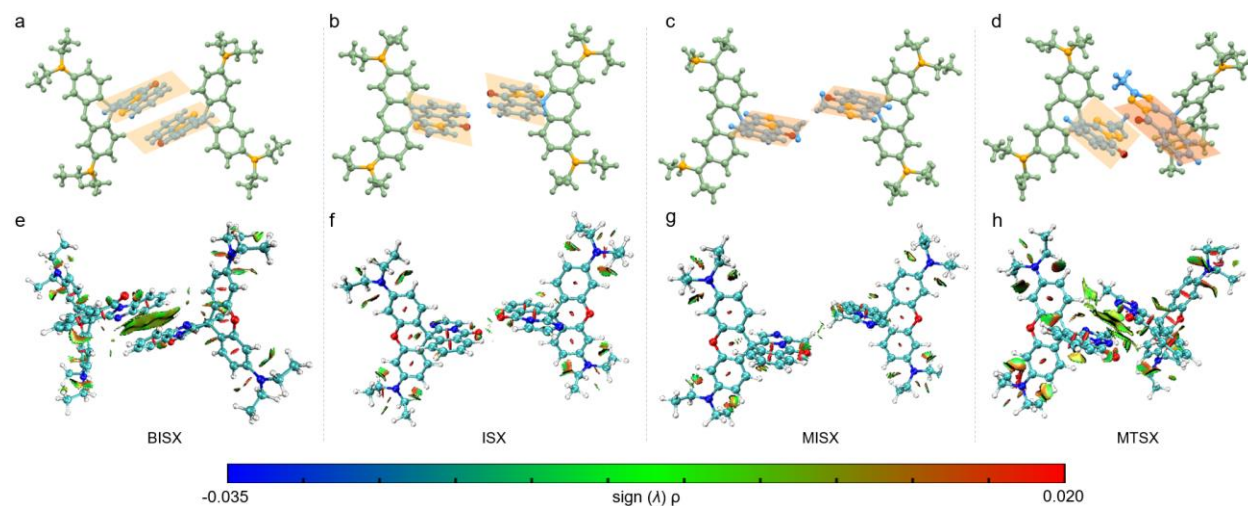
Figure 3. Single-crystal structures (a-d) and reduced density gradient (RDG) analysis (e-h) for dimers of BISX, ISX, MISX and MTSX, respectively. (RDG=0.5).

combining the crystal structure analysis and RDG calculation results, we could conclude that intermolecular through-space interaction is not the fundamental factor in inducing AIE behavior. Since the intermolecular through-space interaction was excluded, we would like to explore other kinds of possibilities that are responsible for the chromophore formation and AIE behavior of these closed-form rhodamines. We doped BISX, ISX, MISX and MTSX into PMMA films with different ratios to restrict their molecular motion, and measured their luminescence properties subsequently (Figure S47 and Figure 4). For BISX, emission intensity of the doping system decreased with a reduced doping ratio from 5% to 0.1% (Figure 4a). Similar results were also found for ISX, MISX and MTSX doped in PMMA film (Figure 4b-d). This suggested that the emission of the four compounds in the isolated state was kind of forbidden even if they were confined in a rigid matrix, while

the aggregation at high concentration can effectively break the transition forbidden to light up the emission. For conventional AIEgens, it is known that both rigidification in the polymeric matrix and reducing environmental temperature can promote the radiative decay rate since molecular motion is restricted, thus providing strong emission. Thus, combined with the previous cooling experimental results, we assumed that except for the RIM mechanism, there may be other reasons for the AIE properties.
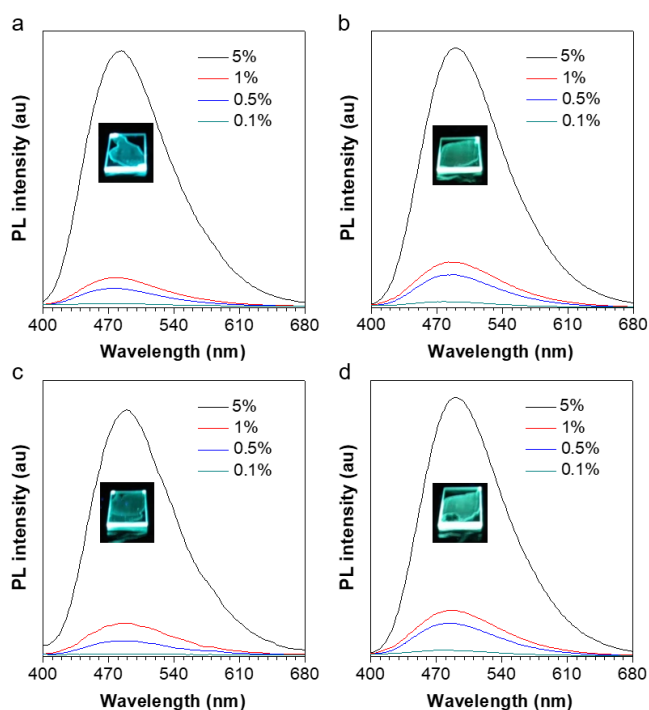
Figure 4. PL spectra of BISX, ISX, MISX and MTSX (a-d) in PMMA film with different weight ratios (m/m), respectively. Inset: fluorescence images of the corresponding compounds in PMMA (5%). λ_{ex} = 365 nm.

Although the four compounds were nonconjugated with donor (D) xanthene and acceptor (A) isoquinolinone parts isolated by an sp^3 carbon atom, intramolecular charge transfer may exist in a through-space way to narrow the band gap, facilitating the chromophore formation. This hypothesis was further supported by theoretical calculation

since the highest occupied molecular orbitals (HOMOs) were distributed on the D moieties (xanthene) while the lowest unoccupied molecular orbitals (LUMOs) were generally distributed on the A moieties (isoquinolinone) as shown in Figure S48. Take BISX for instance, in dilute solutions, the neighboring D and A groups were almost perpendicular to each other with a dihedral angle of 89.5° in the ground state (Figure 5a). Thus, electron clouds of the isolated conjugation rings were not overlapped at all, which has been well recognized as a forbidden factor for electron transition.[58] In the excited state, a relatively smaller dihedral angle of 77.73° was found for the optimized geometry which might allow the electron transition. While in the real case, such large torsion from 89.5° to 77.73° was hard to realize, and the absorbed energy would undergo a non-radiative decay pathway by structural relaxation. Thus, in the solution state, the system was almost non-emissive, most excitons will come to the ground state from the LE state rather than CT excited state, making CT become a dark state (Figure 5a). This diagram also well accounted for the emission behavior of BISX in the previous cooling experiments (Figure 2b-c). At room temperature, due to the flexible molecular motion, the absorbed energy was mainly dissipated via the nonradiative decay pathway, affording negligible LE emission. And the weak CT emission which is responsible for the AIE peak was ascribed to a dark state. Although reducing temperature to restrict the molecular motion benefits enhancing the LE emission at 430 nm, it affects scarcely the forbidden CT emission of the perpendicular D-A structure. However, the aggregation seems to break the transition forbidden of an isolated state since these lightless nonconjugated rhodamine single species emit brightly upon aggregation or crystallization. What happened during the aggregation? Which kind of factors breaks the transition forbidden of molecular species?
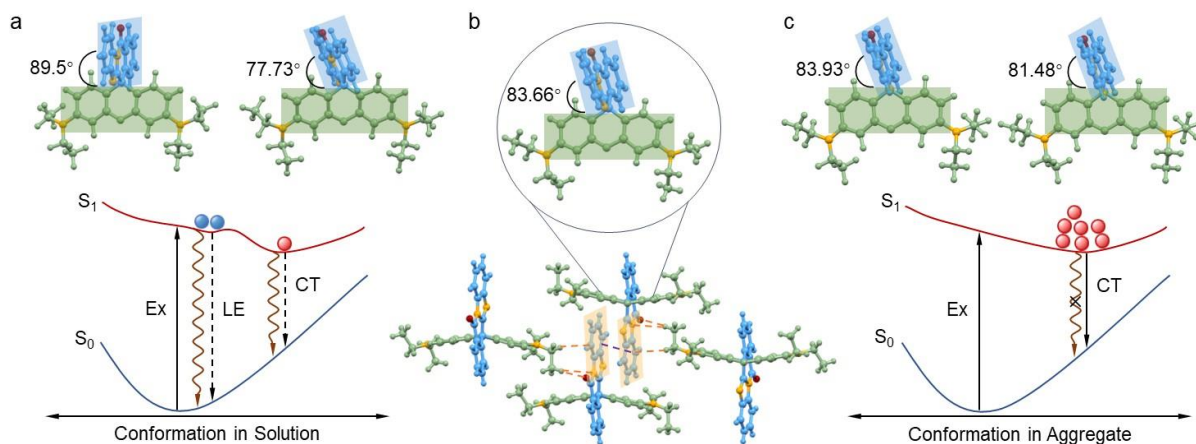
Figure 5. (a) Potential energy surface of BISX in the THF solution and the optimized ground-state and excited-state geometries. (b) Single-crystal structure and packing arrangement of BISX. (c) Potential energy surface of BISX in the crystalline state and the optimized ground-state and excited-state geometries.

To gain deep insight into these questions, theoretical calculations based on single-crystal structures were carried out. In BISX crystals, different from its orthogonal structure in the solution state, a symmetry decreased structure with a smaller D-A dihedral angle of 83.66° within the crystal was observed. Unlike the perpendicular orthogonal structure at freedom state that exhibits almost non-overlapped HOMO and LUMO (Figure S49), the symmetry decrease within the crystal structure leads to an obvious electronic structure change with more effective HOMO and LUMO overlap. The improved HOMO and LUMO overlap benefits effective CT transition to undergo radiative decay. Therefore, the aggregation helps break the transition forbidden in the solution state but facilitates the allowed CT transition in the aggregate state through structural symmetry breaking upon aggregation (Figure 5b and S49). Based on the single-crystal structure, QM/MM calculations were further performed by the ONIOM model in the Gaussian 16 package (Figure S50). As shown in Figure 5c, the variation of the dihedral angle between the

excited state and ground state was merely 2.45°, leading to more accessible structural relaxation to the geometry of allowed CT transition. Thus, in the aggregate state, BISX displayed CT emission at 540 nm. Compared to the high symmetric geometry in the solution state, molecules in the aggregate state were close to each other with various interactions (C-H···π, π-π, hydrogen bonding), which caused a symmetry decreased structure with transition allowed CT emission. Therefore, AIE features of the nonconjugated molecules in our system could be understood from a new viewpoint of aggregation-induced symmetry breaking (AISB). Since symmetry breaking is common in aggregates,[16,17] the highly flexible motion in dilute solutions can be considered as high symmetry of the system, while the restricted motion in the aggregate state can be taken as a decreased symmetry.[18,24,59]

Application in the detection of amines released

Additionally, we checked the PL performance of these nonconjugated rhodamine derivatives in the solid state, respectively. As shown in Figure 6a and 6b, BISX, ISX, MTSX and MISX crystals displayed bright green-blue color fluorescence with emission peaks at 475 nm, 515 nm, 478 nm, and 497 nm, respectively. Their quantum yields were measured as 64.1%, 46.0%, 69.4%, and 72.7%, which are ultrabright visible emissions for these unorthodox nonconjugated structures (Table S2). Notably, we found that the bright fluorescence of BISX was quenched completely when exposed to trifluoroacetic acid (TFA). And the emission recovered when the acid-treated sample was exposed to triethylamine (TEA), as shown in Figure S51a. We assumed introducing TFA protonated the nitrogen atom of BISX (HBISX$^+$), while later TEA treatment made it deprotonation. When further checking the chemical structure of BISX, there are two nitrogen atoms

contained in the conjugation backbone (Figure S51b). The lone pair electrons of the sp^3 nitrogen are perpendicular to the plane of the aromatic ring, forming lone-pair π conjugation, thus the sp^3 N is difficult to be protonated. For the sp^2 N, in the contrast, its lone pair does not participate in conjugated systems, as they are parallel to the molecular plane. The sp^2 hybridized nitrogen is more likely to be protonated. The calculated electron density maps based on electrostatic potential further verified our hypothesis, by giving the result that sp^2 N is more electron-rich than sp^3 N (Figure S51c). We then tested the reversibility and reliability of the system by alternatively exposing the BISX film to TFA and TEA vapors. The bright and dark states could be converted for more than three consecutive cycles with negligible fatigue, revealing the high reversibility and repeatability of this sensor system. Inspired by its "turn-on/ off" response to ammonia vapor after being post-treated with acid, we employed BISX as a food spoilage sensor. We bought fresh clams, crayfish, and fish from the seafood market as detection samples. The fresh seafood was sealed in black-packaged containers with TFA-treated thin films of BISX, and kept at room temperature for 24 h, respectively. After 12 h, faint green emission was observed. After 24 h treatment, the emission became much stronger (Figure 6d). For crayfish and fish, as shown in Figure S52 and S53, the thin film gave a strong green fluorescence when sealed at 12 h, indicating their faster decomposition rate compared to clams. In this regard, food spoilage sensors could be generated for sensitive detection of ammonia and biogenic vapors generated through the food spoilage process.
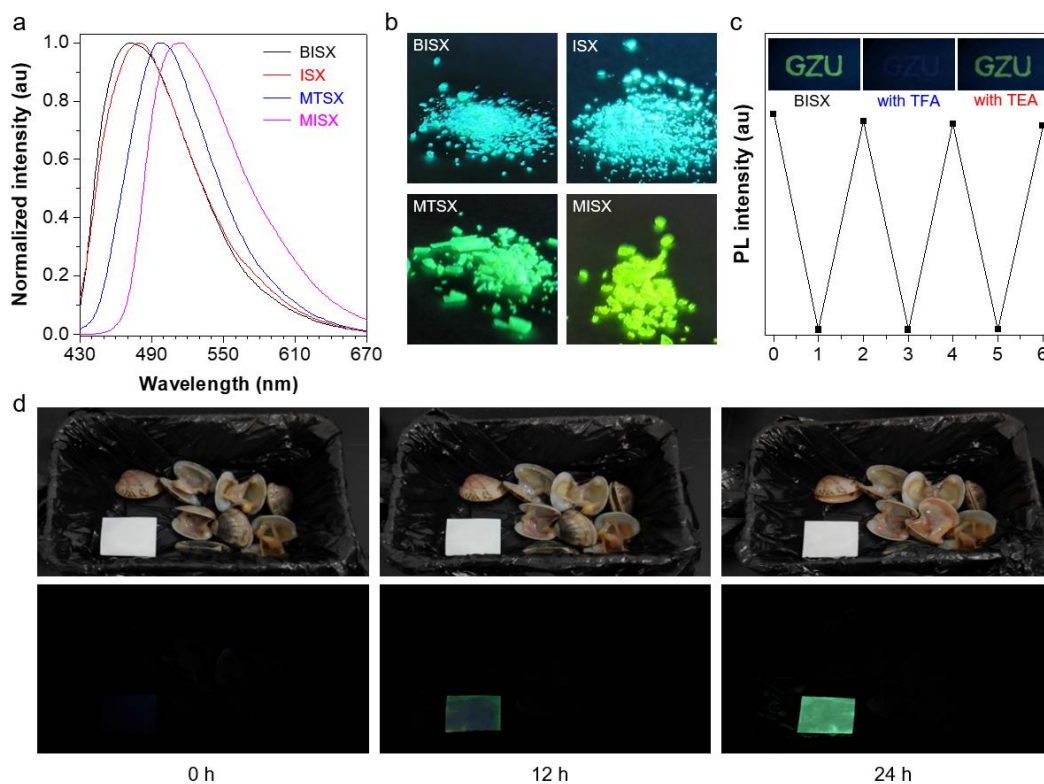
Figure 6. (a) Normalized PL spectra (a) and fluorescence images (b) of BISX, ISX, MISX and MTSX in the aggregate state. λex = 365 nm. (c) Maximal PL intensity of BISX treated with trifluoroacetic acid (TFA) and triethylamine (TEA). Inset: fluorescence images taken under 365 nm UV irradiation, respectively. (d) Spoilage detection of clams in sealed packages for 24 h at room temperature using BISX. Photographs taken under daylight (upper) and 365 nm UV irradiation (bottom).

Discussion

In summary, we synthesized a series of rhodamine-based compounds with novel cross-shaped six-membered structures, namely, BISX, ISX, MISX, and MTSX, *via* a feasible and simple approach based on C–N and C–C coupling cyclization reaction. The compounds displayed typical AIE behavior. While different from conventional AIEgens, their AIE emission intensity did not enhance when increasing viscosity or decreasing temperature, suggesting their AIE properties were not simply attributed to the typical RIM

19

mechanism. Combined with analysis from single-crystal structure, optical properties investigation, and theoretical calculations, we proposed that through-space interactions, resulting from aggregation-induced symmetry breaking, dominated their luminescence variations between solution and aggregation state. When dissolved in THF solutions, molecules in the ground state possessed a transition forbidden orthogonal structure with high symmetry, making it difficult to approach the transition allowed CT excited state. In the aggregate state, however, the ground-state symmetric conformation was broken due to various intermolecular interactions, affording an initial angle for realizing the transition allowed CT excited-state conformation. Besides, taking advantage of the sensitive "turn-on/ off" emission behavior towards acid-base treatment, spoilage detection on seafood was realized. Therefore, aggregation-induced symmetry breaking provides a novel insight for designing unconventional AIEgens. More importantly, it offers a deep understanding of the variations between single molecular and aggregate states.

Methods

General information

All chemicals were purchased from commercial suppliers and used without further purification. The solvents were used as analytic grade during the synthesis of the probes, and the chromatographic grade solvents were used for UV-Vis, and fluorescence instrument tests, etc. Deionized distilled water was used throughout all experiments. All the reactions were magnetically stirred and heated by an oil bath (IKA RCT basic), and thin-layer chromatography (TLC) was Spectrochem GF254 silica gel coated plates. NMR spectra were measured on a JEOL–ECX 500 and Bruker Biospin AG–400 spectrometer at room temperature using TMS as an internal standard. High-resolution Mass

spectrometry (HRMS) spectra were recorded on a Thermo Scientific Q Exactive Quadrupole-Orbitrap mass spectrometer. The crystal data were collected by Bruker Smart Apex II CCD diffractometer. Fluorescence spectra were performed on a PTI QuantaMaster 8000 (Horiba Trading CO., LTD). Fluorescence lifetimes were carried out with FluoroMax-TCSPC (Horiba Trading CO., LTD). Quantum efficiencies were carried out on a PTI QuantaMaster 8000 (Horiba Trading CO., LTD) using an integrating sphere apparatus. UV–Vis spectra were performed on a TU–1900 spectrophotometer. DLS was recorded on DelsaNano C (Beckman Coulter).

Computational Methods

DFT-calculated possible mechanism of MISX reaction: All the calculations were carried out using the Gaussian 16 program package.[60] Single-point energy calculations were then performed on the mechanism using the M06-2X/6-31G (d)[61,62] and PCM solution methods in THF for MISX.

Solution state: BISX, ISX, MISX and MTSX were optimized at M06-2X/6-31G (d) and PCM solution methods in THF. Frequency calculations were performed to confirm the characteristics of all the calculated structures as minima.

Crystal state: BISX was optimized at M06-2X/6-31G (d) in gas. Frequency calculations were performed to confirm the characteristics of all the calculated structures as minima. Subsequently, (TD) M06-2X /6-31G(d) in gas under the Gaussian 16 package.

Aggregate state: We used combined quantum mechanics and molecular mechanics methods (QM/MM). An ONIOM model was constructed by cutting a cluster containing 54

BISX molecules from the single crystal structure to calculate by (TD)M06-2X/6-31G(d) methods in gas under the Gaussian 16 package.

Data availability

The authors declare that the main data supporting the findings of this study are available within the article and its Supplementary Information file. Crystallographic data are available through the Cambridge Crystallographic Data Centre (CCDC), under deposition numbers CCDC 1991171, 2051533-2051534 and 2051536. Extra data are available from the corresponding author upon request.

References

1. Hon, G. The Unnatural Nature of the Laws of Nature: Symmetry and Asymmetry. In *Correspondence, Invariance and Heuristics: Essays in Honour of Heinz Post* (Springer Netherlands: Dordrecht, 1993).

2. Livio, M. Why Symmetry Matters. *Nature* **490**, 472-473 (2012).

3. Katzir, S. The Emergence of the Principle of Symmetry in Physics. *Historical Studies in the Physical and Biological Sciences* **35**, 35-65 (2004).

4. Van Belle, H. Symmetry and Symmetry-Breaking in the Philosophy and Thinking of Leo Apostel. In *World Views and the Problem of Synthesis: The Yellow Book of "Einstein Meets Magritte"* (Springer Netherlands: Dordrecht, 1999).

5. Wang, Z., Xu, W., Liu, L. & Zhu, T. F. A Synthetic Molecular System Capable of Mirror-Image Genetic Replication and Transcription. *Nat. Chem.* **8**, 698-704 (2016).

6. Peplow, M. Mirror-Image Enzyme Copies Looking-Glass DNA. *Nature* **533**, 303-304 (2016).

7. Zhu, X. et al. Negative Phototransistors with Ultrahigh Sensitivity and Weak-Light

Detection Based on 1d/2d Molecular Crystal P–N Heterojunctions and Their Application in Light Encoders. *Adv. Mater.* **34**, 2201364 (2022).

8. Ma, Y.-J., Fang, X., Xiao, G. & Yan, D. Dynamic Manipulating Space-Resolved Persistent Luminescence in Core–Shell Mofs Heterostructures Via Reversible Photochromism. *Angew. Chem. Int. Ed.* **61**, e202114100. (2022).

9. Miao, L.-P. et al. A Ferroelastic Molecular Rotor Crystal Showing Inverse Temperature Symmetry Breaking. *Inorg. Chem. Front.* **8**, 2809-2816 (2021).

10. Yang, X.-G., Zhai, Z.-M., Lu, X.-M., Ma, L.-F. & Yan, D. Fast Crystallization-Deposition of Orderly Molecule Level Heterojunction Thin Films Showing Tunable up-Conversion and Ultrahigh Photoelectric Response. *ACS Cent. Sci.* **6**, 1169-1178 (2020).

11. Schmitt, T. et al. Control of Crystal Symmetry Breaking with Halogen-Substituted Benzylammonium in Layered Hybrid Metal-Halide Perovskites. *J. Am. Chem. Soc.* **142**, 5060-5067 (2020).

12. Walsh, M. J., Tong, W., Katz-Boon, H., Mulvaney, P., Etheridge, J. & Funston, A. M. A Mechanism for Symmetry Breaking and Shape Control in Single-Crystal Gold Nanorods. *Acc. Chem. Res.* **50**, 2925-2935 (2017).

13. Zhang, J. et al. Fullerene/Sulfur-Bridged Annulene Cocrystals: Two-Dimensional Segregated Heterojunctions with Ambipolar Transport Properties and Photoresponsivity. *J. Am. Chem. Soc.* **135**, 558-561 (2013).

14. Kuang, Z., Song, H., Guo, Y., Guo, Q. & Xia, A. Solvent-Induced Symmetry-Breaking Charge Transfer in an Octupolar Triphenylamine Derivative Resolved with Transient Fluorescence Spectroscopy. *Chinese J. Chem. Phy.* **32**, 59-66 (2019).

15. Beckwith, J. S. et al. Specific Monitoring of Excited-State Symmetry Breaking by

Femtosecond Broadband Fluorescence Upconversion Spectroscopy. *J. Phy. Chem. Lett.* **8**, 5878-5883 (2017).

16. Dereka B*, et al.* Solvent tuning of photochemistry upon excited-state symmetry breaking. *Nat. Commun.* **11**, 1925 (2020).

17. Landau, L. D. On the Theory of Phase Transitions. *Zh.Eksp.Teor.Fiz.* **7**, 19-32 (1937).

18. Landau, L. D. The Theory of Phase Transitions. *Nature* **138**, 840-841 (1936).

19. Zhang, H. et al. Aggregate Science: From Structures to Properties. *Adv. Mater.* **32**, e2001457 (2020).

20. Mei, J., Leung, N. L. C., Kwok, R. T. K., Lam, J. W. Y. & Tang, B. Z. Aggregation-Induced Emission: Together We Shine, United We Soar! *Chem. Rev.* **115**, 11718-11940 (2015).

21. Wang, H. et al. Visualization and Manipulation of Solid-State Molecular Motions in Cocrystallization Processes. *J. Am. Chem. Soc.* **143**, 9468-9477 (2021).

22. Li, S. & Yan, D. Two-Component Aggregation-Induced Emission Materials: Tunable One/Two-Photon Luminescence and Stimuli-Responsive Switches by Co-Crystal Formation. *Adv. Opt. Mater.* **6**, 1800445 (2018).

23. Turner, M. J., Thomas, S. P., Shi, M. W., Jayatilaka, D. & Spackman, M. A. Energy Frameworks: Insights into Interaction Anisotropy and the Mechanical Properties of Molecular Crystals. *Chem. Commun.* **51**, 3735-3738 (2015).

24. Qian, Q., Nakamura, J., Fallahi, S., Gardner. G. C., & Manfra, M. J. Possible nematic to smectic phase transition in a two-dimensional electron gas at half-filling. *Nat. Commun.* **8**, 1536 (2017).

25. Zhan, L. et al. A Simple Organic Molecule Realizing Simultaneous Tadf, Rtp, Aie, and

Mechanoluminescence: Understanding the Mechanism Behind the Multifunctional Emitter. *Angew. Chem. Int. Ed.* **58**, 17651-17655 (2019).

26. Ma, S., Du, S., Pan, G., Dai, S., Xu, B. & Tian, W. Organic Molecular Aggregates: From Aggregation Structure to Emission Property. *Aggregate* **2**, e96 (2021).

27. Nishiuchi, T., Sotome, H., Fukuuchi, R., Kamada, K., Miyasaka, H. & Kubo, T. Optical Nature of Non-Substituted Triphenylmethyl Cation: Crystalline State Emission, Thermochromism, and Phosphorescence. *Aggregate* **2**, e126 (2021).

28. Li, Y. *et al*. Metallacycle/Metallacage-Cored Fluorescent Supramolecular Assemblies with Aggregation-Induced Emission Properties. *Adv. Opt. Mater.* **8**, 1902190 (2020).

29. Zhang, P., Zhang, J., Xue, Z., Wang, J. & Jiang, L., Reliable Manipulation of Gas Bubbles by Regulating Interfacial Morphologies and Chemical Components. *Mater. Horiz.* **4**, 665-672 (2017).

30. Luo, J. *et al*. Aggregation-Induced Emission of 1-Methyl-1,2,3,4,5-Pentaphenylsilole. *Chem. Commun.* 1740-1741 (2001).

31. Zhao, Z. *et al.* Non-Aromatic Annulene-Based Aggregation-Induced Emission System Via Aromaticity Reversal Process. *Nat. Commun.* **10**, 2952 (2019).

32. Zhang, J., Zhang, H., Lam, J. W. Y. & Tang, B. Z. Restriction of Intramolecular Motion(Rim): Investigating Aie Mechanism from Experimental and Theoretical Studies. *Chem. Res. Chinese U.* **37**, 1-15 (2021).

33. Peng, Q. & Shuai, Z. Molecular mechanism of aggregation‐induced emission. *Aggregate* **2**, e91 (2021).

34. Tu, Y. Zhao, Z. Lam, J. W. Y. & Tang, B. Z. Aggregate Science: Much to Explore in the Meso World. *Matter* **4**, 338-349 (2021).

35. Zhao, Z. Zhang, H. Lam, J. W. Y. & Tang, B. Z. Aggregation-Induced Emission: New Vistas at the Aggregate Level. *Angew. Chem. Int. Ed.* **59**, 9888-9907 (2020).

36. Turley, A. T. *et al.* Extended Conjugation Attenuates the Quenching of Aggregation‐Induced Emitters by Photocyclization Pathways. *Angew. Chem. Int. Ed.* e202202193 (2022).

37. Huang Y, et al. Reducing aggregation caused quenching effect through co-assembly of PAH chromophores and molecular barriers. *Nat. Commun.* **10**, 169 (2019).

38. Wang, H. *et al.* Positive/Negative Phototropism: Controllable Molecular Actuators with Different Bending Behavior. *CCS Chem.* **3**, 1491-1500 (2021).

39. Li, Q. et al. Unusual Light-Driven Amplification through Unexpected Regioselective Photogeneration of Five-Membered Azaheterocyclic Aiegen. *Chem. Sci.* **12**, 709-717 (2021).

40. Li, Q. et al. Time-Dependent Photodynamic Therapy for Multiple Targets: A Highly Efficient Aie-Active Photosensitizer for Selective Bacterial Elimination and Cancer Cell Ablation. *Angew. Chem. Int. Ed.* **59**, 9470-9477 (2020).

41. Zhu, H., Li, Q., Zhu, W. & Huang, F. Pillararenes as Versatile Building Blocks for Fluorescent Materials. *Acc. Mater. Res.* **3**, 658-668 (2022).

42. Feng, H.-T., Liu, C., Li, Q., Zhang, H., Lam, J. W. Y. & Tang, B. Z. Structure, Assembly, and Function of (Latent)-Chiral Aiegens. *ACS Mater. Lett.* **1**, 192-202 (2019).

43. Feng, J. et al. Acid Stimuli Responsive Cpl from Supramolecular Assembly of Aie Molecule. *J. Phy. Chem. C* **125**, 21270-21276 (2021).

44. Zhang M-M, *et al.* AIE Triggers the Circularly Polarized Luminescence of Atomically Precise Enantiomeric Copper(I) Alkynyl Clusters. *Angew. Chem. Int. Ed.* **59**, 10052-

10058 (2020).

45. Liu, D. *et al.* Organic Laser Molecule with High Mobility, High Photoluminescence Quantum Yield, and Deep-Blue Lasing Characteristics. *J. Am. Chem. Soc.* **142**, 6332-6339 (2020).

46. Shi X*, et al.* Hierarchical Supramolecular Self-Assembly: Fabrication and Visualization of Multiblock Microstructures**. *Angew. Chem. Int. Ed.* **61**, e202211298 (2022).

47. Gong J*, et al.* ASBase: The universal database for aggregate science. *Aggregate.* **n/a**, e263 (2022).

48. Anderson, P. W. More Is Different. *Science* **177**, 4047 (1972).

49. Yu, M.-X. *et al.* White-Light Emission and Circularly Polarized Luminescence from a Chiral Copper(I) Coordination Polymer through Symmetry-Breaking Crystallization. *Angew. Chem. Int. Ed.* **61**, e202201590 (2022).

50. Dhbaibi, K. *et al.* Modulation of Circularly Polarized Luminescence through Excited-State Symmetry Breaking and Interbranched Exciton Coupling in Helical Push–Pull Organic Systems. *Chem. Sci.* **11**, 567-576 (2020).

51. Lardon, N. *et al.* Systematic Tuning of Rhodamine Spirocyclization for Super-Resolution Microscopy. *J. Am. Chem. Soc.* **143**, 14592-14600. (2021).

52. Wang, L., Du, W., Hu, Z., Uvdal, K., Li, L. & Huang, W. Hybrid Rhodamine Fluorophores in the Visible/Nir Region for Biological Imaging. *Angew. Chem. Int. Ed.* **58**, 14026-14043 (2019).

53. Ma, Z. *et al.* A Mechanochromic Single Crystal: Turning Two Color Changes into a Tricolored Switch. *Angew. Chem. Int. Ed.* **55**, 519-522 (2016).

54. Chen, Y. *et al.* Aiegens for Dark through-Bond Energy Transfer: Design, Synthesis,

Theoretical Study and Application in Ratiometric Hg(2+) Sensing. *Chem. Sci.* **8**, 2047-2055 (2017).

55. Li, Y. *et al.* A Single Crystal with Multiple Functions of Optical Waveguide, Aggregation-Induced Emission, and Mechanochromism. *ACS Appl. Mater. Interfaces* **9**, 8910-8918 (2017).

56. Yang, L.-L., Tang, A. L., Wang, P.-Y. & Yang, S. Switching of C–C and C–N Coupling/Cleavage for Hypersensitive Detection of Cu2+ by a Catalytically Mediated 2-Aminoimidazolyl-Tailored Six-Membered Rhodamine Probe. *Org. Lett.* **22**, 8234-8239. (2020).

57. Wang, H. *et al.* "Living" Luminogens: Light Driven Acq-to-Aie Transformation Accompanied with Solid-State Actuation. *Mater. Horiz.* **7**, 1566-1572 (2020).

58. Grabowski, Z. R., Rotkiewicz, K. & Rettig, W. Structural Changes Accompanying Intramolecular Electron Transfer: Focus on Twisted Intramolecular Charge-Transfer States and Structures. *Chem. Rev.* **103**, 3899-4032 (2003).

59. Prigogine I, Nicolis G. Self-Organisation in Nonequilibrium Systems: Towards A Dynamics of Complexity. In: *Bifurcation Analysis: Principles, Applications and Synthesis* (eds Hazewinkel M, Jurkovich R, Paelinck JHP). Springer Netherlands (1985).

60. Frisch, M. J. *et al. Gaussian 16, Revision A.03*, Gaussian, Inc., Wallingford, CT (2016).

61. Zhao, Y. & Truhlar, D. G., Density Functionals with Broad Applicability in Chemistry. *Acc. Chem. Res.* **41**, 157-167 (2008).

62. Zhao, Y. & Truhlar, D. G., The M06 suite of density functionals for main group thermochemistry, thermochemical kinetics, noncovalent interactions, excited states,

and transition elements: two new functionals and systematic testing of four M06-class functionals and 12 other functionals. *Theor. Chem. Acc.* **120**, 215-241 (2008).